

NEURAL NETWORKS FOR BVI SYSTEM IDENTIFICATION

Holger Gläßel¹, Jan Kahl², Oliver Dieterich², Stephan Rudolph¹

¹ Institut für Statik und Dynamik der Luft- und Raumfahrtkonstruktionen, Universität Stuttgart, Germany,

² Eurocopter Deutschland GmbH, Ottobrunn, Germany

The BO105 IBC demonstrator of EUROCOPTER Deutschland (ECD) has shown the successful application of 2/rev blade root actuation for significant blade vortex interaction (BVI) noise reduction during flight tests. In order to evaluate and assess advanced BVI noise control concepts, plant models are required for a sophisticated controller design. However, modelling the dynamic behaviour of the plant based on extensive CFD calculations is practically not feasible. Due to their special capabilities with respect to non-linear behaviour, the selection of neural networks for this kind of modelling task is a reasonable alternative.

The paper focuses on the application of neural networks for BVI system identification purposes, presenting an overview of combined research activities by the "Institut für Statik und Dynamik der Luft- und Raumfahrtkonstruktionen (ISD)" and ECD. Two methodologies are outlined to achieve this goal:

On the one hand a black box approach is used, whereby neural networks are trained to reproduce the pressure output of a specific Kulite that was gathered during the open loop flight test campaign in 1998. Based on the assumption of plant periodicity, a system identification approach is discussed using series of small neural networks for the representation of one rotor revolution. The clustered networks show good mapping ability concerning the interpolation of pressure data for various IBC phase angles.

On the other hand, a grey box approach comprises physical knowledge about the mechanism of BVI, including a simplified model of the tip vortex convection similar to prescribed wake models. The above mentioned blade pressure data is filtered to extract the position and strength of interactions. Several neural network modules map different aspects of the vortex wake and are adapted to predict the occurring BVI events as a whole. Each of these neural modules do thereby keep their physical interpretation.

The current state of the results is presented and discussed. The identified neural plant models have the potential to be efficiently applied for real time applications i.e. in-flight BVI control.

Nomenclature

BVI	Blade Vortex Interaction
CFD	Computational Fluid Dynamic
ECD	Eurocopter Deutschland
DNW	Deutsch-Niederländischer Windkanal
IBC	Individual Blade Control
ISD	Institut für Statik und Dynamik der Luft- und Raumfahrtkonstruktionen
NN	Neural Network
TPP	Tip Path Plane
A	higher harmonic amplitude
\dot{A}	time-variant harmonic amplitude
CW	wavelet coefficient
a, c, h	parameter of Mangler inflow
C, H	parameter of IBC inflow
f	wavelet frequency
k_x	longitudinal inflow gradient
m	adjacent harmonics
N	number of rotor blades
p_i	pressure sample
r	radial coordinate
R	blade radius
rev	rotor revolution
s	(flight) state
t	time
u	system input
x, y, z	TPP coordinate system

α_{TPP}	TPP angle of attack
ΔC_p	BVI pressure rise
φ	IBC phase shift
λ	rotor inflow ratio
λ_i	induced inflow ratio
λ_{i0}	mean induced inflow ratio
μ	advance ratio
μ_z	axial advance ratio
Ω	rotor rotational frequency
θ_{IBC}	local IBC pitch input
ψ	rotor azimuth

Indices

n	multiple of rotor frequency $\Omega (n/rev)$
w	vortex wake
wa	wake age
$w0$	vortex at origin

1 Introduction

Exterior helicopter noise is one of the most stringent challenges for helicopter designers today. It significantly limits the operational envelope of helicopters for various applications e.g. for commuter services in the vicinity of densely populated areas. One of the most annoying noise

phenomena is blade vortex interaction (BVI) noise, typically occurring during descent flight and thereby increasing the noise emission on ground due to the low altitude before landing. Numerous efforts have been undertaken in order to reduce BVI noise emission by adequate design of the main rotor blades. Nevertheless, rotor blade design is a multi-objective optimisation and optimised blade designs must not show deficiencies in other fields e.g. performance or control loads leading to severe boundary conditions with respect to design issues. Taking into account today's technology, the potential of BVI noise reduction by passive means seems not to meet the requirements for a wide-spread use of helicopters in urban areas.

A promising alternative approach for significant BVI noise reduction is found in the application of active rotor control technologies. Both wind tunnel and flight test campaigns have demonstrated the effectiveness of applying higher harmonic blade pitch variations under flight conditions with high BVI occurrence. Regarding these test campaigns the higher harmonic pitch input was realised either by actuating the swashplate in the fixed frame with multiples of the main rotor rotational frequency or by hydraulic actuators replacing the pitch links in the rotating system. While the harmonic actuation of the swashplate – often designated as higher harmonic control (HHC) – is limited to $i \cdot N/rev$ and $i \cdot (N \pm 1)/rev$, $i = 1, 2, 3, \dots$ for a N -bladed rotor system due to the limited degrees of freedom offered by the swashplate system, the individual blade control (IBC) allows the independent control of each blade. Due to blade pitch variations, both systems affect BVI noise characteristics mainly by modifying the inflow conditions in the vicinity of the rotor disk.

In 1991, a dynamically scaled model of the four bladed BO105 main rotor was tested in the German-Dutch wind tunnel DNW as cooperative research effort on HHC by the "Deutsches Zentrum für Luft- und Raumfahrttechnik" (DLR), the NASA Langley research centre, Eurocopter Germany (formerly MBB) and Eurocopter (formerly Aerospatiale) (Ref 1). The experimental activities revealed that the BVI noise level can be reduced significantly by HHC input but the most beneficial HHC settings also lead to an increase of vibrations.

In 1990 and 1991, first flight tests on a BO105 helicopter equipped with blade root actuation showed some promising results regarding BVI by IBC, although for safety reasons pitch control authority was limited. In order to examine the full potential of IBC, a full scale BO105 main rotor incorporating an improved IBC system was tested in 1993 and 1994 in the 40 by 80 ft NASA Ames wind tunnel (Ref 2). Extensive tests in single frequency mode (defined by amplitude, frequency and phase angle) demonstrated the effectiveness of $2/rev$ and $3/rev$ IBC inputs. Furthermore, side effects of $2/rev$ IBC on vibration were found to be not as severe as

obtained by the application of $3/rev$ pitch control. Nevertheless, the phase angle of optimal BVI noise suppression depends on the flight conditions. As a consequence of that - an optimised IBC input for one flight condition may lead to an increase of BVI noise for another flight condition - effective BVI noise reduction by IBC requires the usage of a closed loop system.

In 1998, flight tests of the IBC equipped BO105 helicopter were performed by Eurocopter Deutschland in order to confirm the wind tunnel test results (Ref 3). Main differences between wind tunnel tests and flight tests are seen in the presence of tail rotor and engine noise regarding the flight tests, in the trim conditions leading to different hub moments and in the weather conditions providing a realistic scenario. Although the flight tests were performed in the open loop mode (mostly $2/rev$), the test campaign represents a major step towards BVI closed loop control due to the complex data acquisition systems on ground and on board answering questions regarding the appropriate sensor system for feedback control. The neighbourhood noise was measured by a ground-based microphone array consisting of 11 ground microphones arranged up to 300 m on both sides of the flight path and 3 microphones on tripods according to ICAO noise certification rules. The helicopter was equipped with five pressure transducers on the leading edge of one main rotor blade in order to detect impulsive pressure changes due to BVI. Furthermore, microphones were installed on both sides on the helicopter landing skids. Good correlations were obtained between noise reduction measured simultaneously by ground microphones and by skid microphones. Furthermore, the blade pressure data shows the avoidance of pressure peaks related to BVI in consistency to the microphone measurements by selecting appropriate IBC inputs.

The IBC flight test campaign was continued with the application of BVI closed loop control (Ref 4). The investigated noise control concept is based on BVI index minimisation by applying $2/rev$ IBC input. Due to the optimisation of the IBC phase by the "Golden Section Rule" (a gradient free procedure for searching minima), only a very limited knowledge of the helicopter BVI noise characteristics is required for the design of the controller. Two different controllers were applied, the first one only controlling the IBC phase by fixed IBC amplitude and the second one controlling both IBC phase and amplitude. Both controllers showed adequate results in BVI noise reduction during standard descent flight conditions in consistency with the open loop flight test campaigns performed earlier. Nevertheless, transient manoeuvres showed that the application of the Golden Section Rule slows down controller response. Although a certain potential of improving the two controllers is identified by optimising controller parameters, other concepts are analysed at Eurocopter Deutschland, promising good

performance under transient conditions by inclusion of additional knowledge into the controller with respect to helicopter BVI noise characteristics.

From a control point of view, the dynamic plant model required for sophisticated controller design is of high non-linearity since a high frequency phenomenon – the BVI noise as system output higher than $20/rev$ – should be controlled by low frequency input – $2/rev$ IBC or similar. A theoretical derivation of an adequate dynamic plant model seems practically not feasible with today's knowledge. Therefore, system identification methods are analysed for generating BVI plant models based on flight test data. Due to their special capabilities with respect to non-linear behaviour, neural networks appear to be a very attractive alternative for this kind of purpose.

2 Neural Networks for Modelling

Neural networks (NN) allow a data driven design of linear and non-linear mappings represented by means of many input and output data samples. Especially in the case of an unknown analytical relation between inputs and outputs, i.e. a missing mathematical description of the system behaviour, experimental data is often the only source of knowledge. Providing representative data samples, neural networks show the potential to adapt to the underlying function. Considering the large amount of in-flight measurements, neural networks seem to be well suited for the identification of the BVI system. In addition, they perform a highly parallel and therefore fast computation which is demanded when using them as a real time plant model.

Basically, neural networks consist of small computational units called neurons, which form a network using weighted connections between different layers. By selecting an appropriate activation function within the neurons, neural networks can perform linear as well as non-linear mappings (Ref 5). The weights of the network connections are free parameters which are adapted during the learning process so that the output error is minimized. Different learning algorithms are available in standard software packages, such as MATLAB (Ref 6), which has been used in this work.

The behaviour of neural networks can be influenced by means of different network topologies. Two main types can be distinguished, feed forward and recurrent networks. Recurrent networks allow backward connections (loops), being dynamic systems they may become unstable, while feed forward networks are static systems and can be proven to be unconditionally stable. Nevertheless, it is possible to perform dynamic mappings with feed forward networks as well, providing time delayed inputs according to the order of the dynamic system (Ref 7).

Since no general rules for choosing an appropriate network architecture exist, the design of a neural model is an iterative procedure finding a trade-off between the network structure i.e. activation function, number and size of layers and the mapping quality. However, certain limits on the choice of an appropriate topology, size and generalisation properties of a non-linear feed forward NN do exist based on proven engineering principles (Ref 8).

In the following chapters, two different approaches for BVI system identification are presented. While the black box approach is based only on the flight test database, a more sophisticated grey box approach additionally incorporates physical knowledge in the identified BVI plant model.

3 Black Box Approach

During the IBC flight test campaign in 1998 with focus on $2/rev$ open loop mode, a large amount of experimental data was acquired. On the leading edge of one main rotor blade five pressure probes (Kulite elements) with different radial positions measured the local blade pressure occurring during flight. The acquired pressure signals show the appearance of BVI by a series of high frequency pressure peaks on the advancing and retreating rotor side in dependence of the flight state and of the IBC input. Thus, the occurrence of BVI can be identified optically or by means of an appropriate index number. Therefore, the pressure signals represent a suitable medium for system identification regarding the BVI phenomenon.

The pressure signals were processed with a sampling rate of 512 per revolution, meaning that every revolution of the rotor blade is discretised with $360^\circ/512 = 0,703^\circ$ rotor azimuth increments. For the flight conditions, performed during the flight tests with emphasis on a 6° descent at 60 KTAS, the pressure value of one sample position p_i is assumed to be constant leading to a periodic discrete function

$$p_i = p_{i+512 \cdot rev}, \quad rev = 1, 2, 3, \dots \quad (3.1)$$

Disturbances due to turbulence, pilot inputs etc. are not taken into account at the moment by using selected rotor revolutions as representatives. Thus, for the investigated flight state, the pressure value at a selected sample position depends only on the control input u

$$p_i = p_i(u) \quad (3.2)$$

If adequate data for additional flight states s is provided, this functionality can be expanded to

$$p_i = p_i(u, s) \quad (3.3)$$

Regarding this fact it sounds reasonable to select a cluster of 512 small feed forward neural networks, one network for each sample position, as can be seen in Fig 1. Each network is trained separately with the matching data at that position. The output of

the networks has to be regarded consecutively to obtain a discrete pressure signal covering one main rotor revolution.

3.1 Training Data

The acquired data consists of pressure signals for different IBC phases φ . Due to efficiency reasons an amplitude A of 1° was applied during the flight test campaign. The resulting local IBC pitch input is defined by

$$\theta_{IBC} = A \cos(\Omega t - \varphi) \quad (3.4)$$

According to the flight tests the different phases for the model inputs are selected from 0° up to 330° in 30° steps including an additional reference case without any IBC input. Thus, 13 different IBC cases are available in total for the investigated flight attitude.

The training by backpropagation of the feed forward networks is done by presenting an input value and a matching output value. The system input u is determined to be of the form $A \sin \varphi$ and $A \cos \varphi$. Thus, the following definition seems to be adequate for a periodic structure of the system input

$$u = \begin{bmatrix} A \sin(\varphi) \\ A \cos(\varphi) \end{bmatrix} \quad (3.5)$$

For constant IBC phase and amplitude the model input u is constant and the same for all 512 networks (Fig 1). As output data the matching flight test pressure data is taken. For these investigations the pressure transducer on 87% radial station is used. The signals of the other radial stations show similar behaviour. The training samples are provided to the networks in matrix form, i.e. batch training is applied.

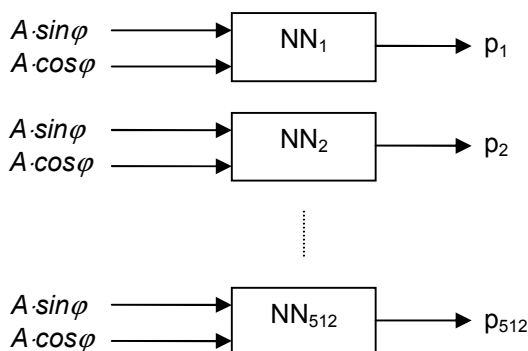


Fig 1: Cluster of 512 networks producing the pressure output of one rotor revolution.

3.2 Network Structure

For the limiting amount of 13 different training cases only small neural networks with a few free parameters (weights) lead to adequate results. Investigations with different kinds of networks have

demonstrated that networks with two layers show appropriate performance. Although one neuron in the output layer is obligatory because of the single output, the number of neurons in the first layer can be different from the number of inputs. Two and three neurons in the first layer (see Fig 2) proved to be a good solution but also larger networks have been investigated. The non-linear behaviour of the neural network is totally contained in the first layer using a non-linear, sigmoid activation function. The output layer as linear function maps the value into the physical space.

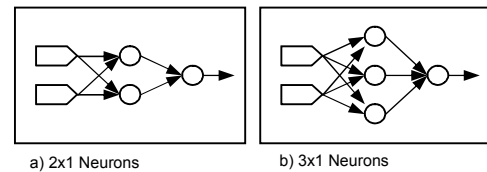


Fig 2: Feed forward networks with 2 (a) and 3 (b) hidden neurons.

The used algorithm for training was the well known Levenberg-Marquardt (Ref 6) algorithm. Additionally the Bayesian Framework Regularization (Ref 6) was applied in order to prevent overfitting.

3.3 Results

The trained cluster of networks is able to reproduce the pressure signal adequately for the case without IBC, as shown in Fig 3, although the pressure signal is highly non-linear.

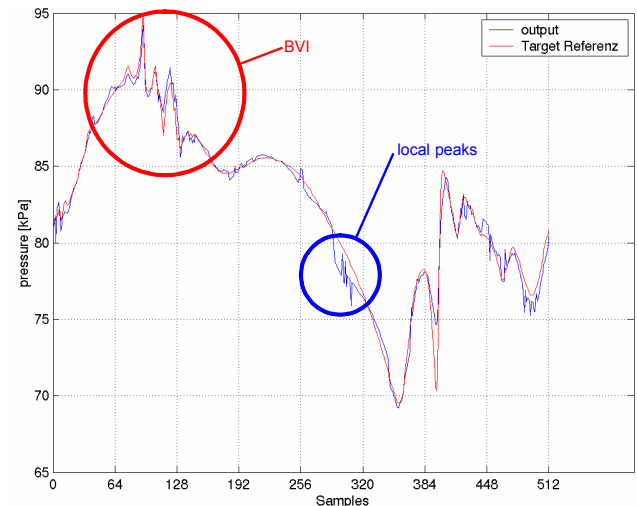


Fig 3: Pressure signal without IBC input (blue: network output, red: flight test data), marked with a red circle is the BVI phenomenon, marked with a blue circle are local peaks.

Compared is a pressure signal of test flight data (training target) to the network output. As expected for this flight case, the BVI phenomenon in the form of pressure peaks occurs on the advancing side and can be clearly identified between samples 64 and 128. The result shows good overall behaviour. The

local spikes in the signal (see Fig 3 between sample 256 and 320) can be explained with the missing information flow between the sample positions as discussed later.

Fig 4 shows the results of a flight state with IBC enabled using 60° phase. The output shows a similar behaviour as in Fig 3. Local spikes are still present but on different sample positions. The previously perceivable BVI between samples 64 and 128 does no longer occur due to IBC inputs.

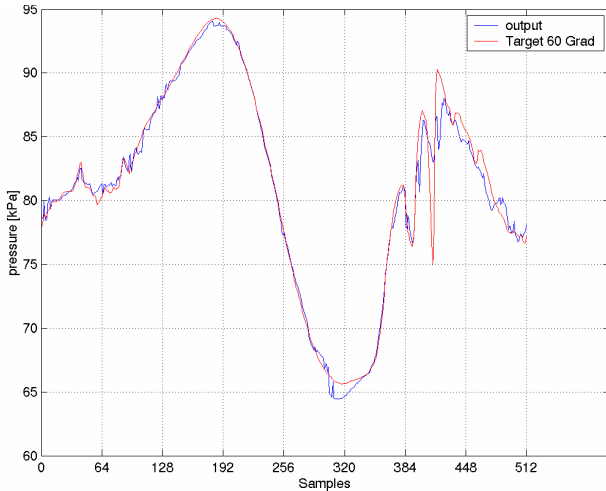


Fig 4: Pressure signal with IBC input $\varphi = 60^\circ$ (blue: network output, red: flight test data).

To show the ability to interpolate between learned IBC cases, intermediate cases are simulated and compared to the nearest available flight data cases. Fig 5 depicts the simulated 75° IBC case together with the 60° and the 90° phase. The network delivers an output that is settled in between the original data.

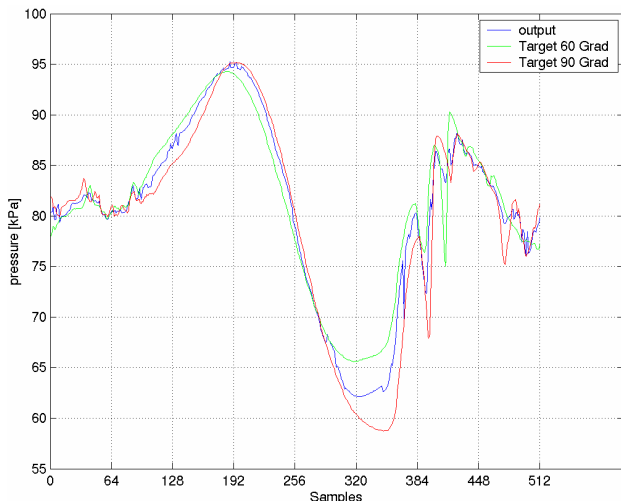


Fig 5: Pressure signal with IBC input $\varphi = 75^\circ$ (blue: network output, green: flight test data $\varphi = 60^\circ$, red: flight test data $\varphi = 90^\circ$).

The output for this interpolated case is consistent with Fig 3 and Fig 4. Concerning the general

behaviour and occasional spikes the signal lies in between the neighbour signals $\varphi = 60^\circ$ and 90° .

Regarding these results it can be recognised that the network output has a more rough character including spikes. This can be explained by the fact that no information is exchanged or no information flow takes place between the networks. Every network is trained and simulated autonomously without regard to its neighbours. Thus, no inherent smoothing mechanism is acting in azimuth direction.

3.4 Merging of Networks

To overcome the problem of missing information flow between the small networks, a modification of the neural network structure was performed by merging the small networks into bigger ones. Step by step two adjacent networks were united resulting in one network with the same input vector, but the number of outputs is doubled representing consecutive samples. For 512 samples per revolution, this procedure can be applied nine times finally resulting in a single network with 512 outputs representing the entire rotor revolution. This procedure is shown in Fig 6 a) to c).

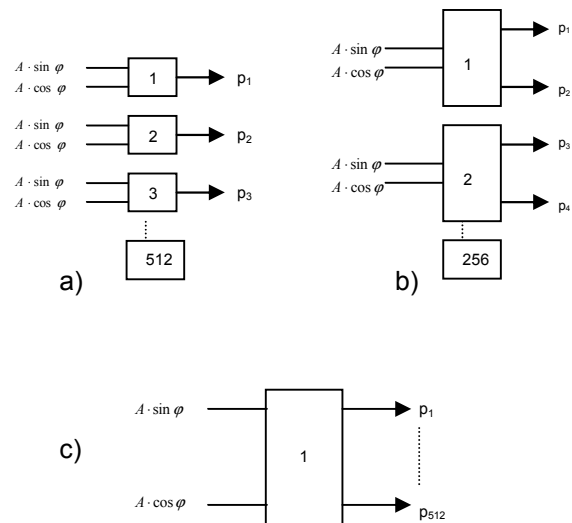


Fig 6: Three different network clusters:
a) 512 networks, b) 256 networks each with 2 outputs, c) one network with 512 outputs

Using one neuron in the output layer for every output, the network becomes large and thus, time to perform training increases exponentially. For the IBC case $\varphi = 60^\circ$ the output of this network is shown in Fig 7. The pressure signal is visibly more smooth but it is possible that BVI, resulting in pressure peaks, is not reproduced properly any more.

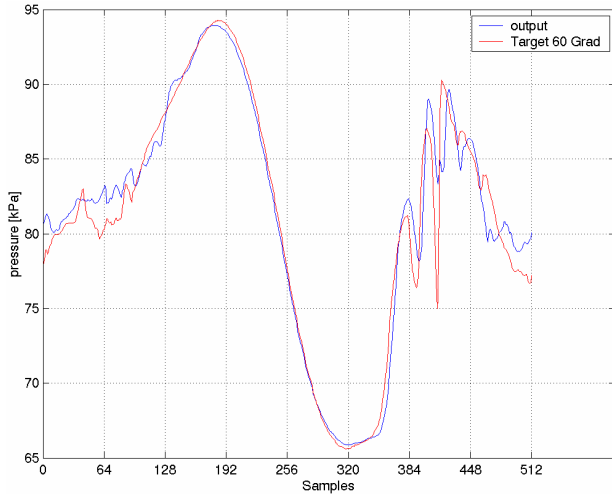


Fig 7: Pressure signal with IBC phase $\varphi = 60^\circ$ (blue: network output, red: flight test data).

3.5 BVI Index

To analyse the quality of the networks, an objective comparison of BVI resulting from the predicted and the measured pressure signals has to be performed. Therefore, a BVI index according to (Ref 9) is used to evaluate the occurring interactions. It is defined as the integral of the coefficients CW resulting from a wavelet analysis

$$BVIX = \frac{1}{\Delta\psi\Delta f\Delta r} \int_{r_1}^{r_2} \int_{f_1}^{f_2} \int_{\psi_1}^{\psi_2} CW(\psi, f, r) d\psi df dr \quad (3.6)$$

The BVI index is implemented in discrete form replacing the integral by finite sums over the azimuth ψ , the wavelet frequency f and the rotor radius r . Fig 8 shows how the BVI index is affected by the size of the networks for the 90° IBC case.

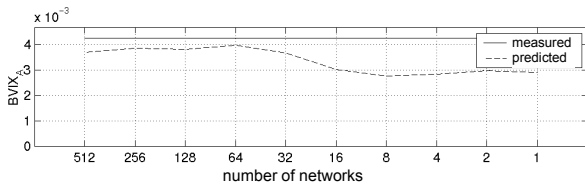


Fig 8: Variation of BVI index for different network sizes, IBC input $\varphi = 90^\circ$ (solid: based on test flight data, dashed: based on network output).

The BVI indices calculated from the outputs of the different sized clusters of networks are smaller than the index from the flight test data. The rough character of the small networks does not result in a high BVI index. The expected suppression of BVI in the bigger networks can be seen in Fig 8 beginning from 64 single networks per cluster and getting stronger.

3.6 Transient Simulation

To evaluate the generalisation of the network outputs for embedding the neural plant model into a controller design, a procedure is implemented to simulate the different kinds of network clusters with time dependent input data. As representative case the simulation of a rising amplitude is discussed. The inputs $A \sin \varphi$ and $A \cos \varphi$ are arranged with an amplitude changing from zero to one in several revolutions rev

$$u(t) = \begin{bmatrix} \tilde{A}(t) \sin \psi \\ \tilde{A}(t) \cos \psi \end{bmatrix} \quad (3.7)$$

$$\tilde{A}(t) = A \cdot \frac{i}{512 \cdot rev}, \quad A = 1^\circ, \quad 0 < i < 512 \cdot rev \quad (3.8)$$

The pressure signal is changing continuously from one IBC state to the other (Fig 9). Although no pressure signals are available for such IBC inputs, the simulation results depict a smooth and reasonable change. Additionally, the BVI index, separately calculated for each rotor revolution, is shown below the respective interval. It shows a constant change from one case to the other as well. As expected, the BVI index is decreased by engaging IBC control, visible by the disappearance of the peaks on the advancing side.

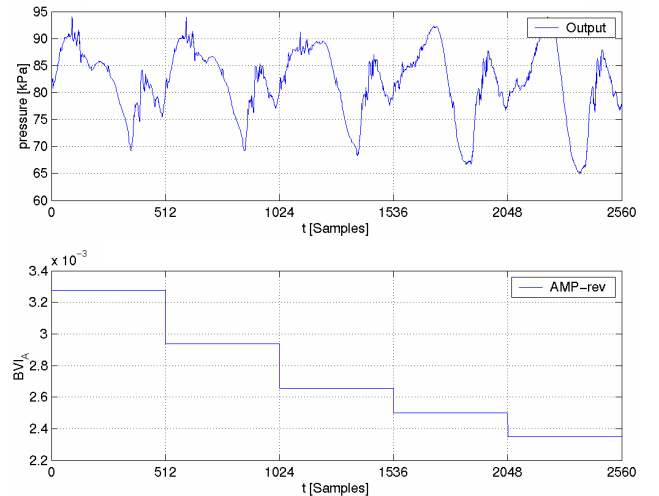


Fig 9: Simulation of increasing IBC amplitude (above: network output, below: BVI index).

3.7 Discussion

The investigated networks are capable of depicting the complex rotor system behaviour in terms of highly non-linear pressure signals for enabled and disabled IBC input. Due to implemented stationary behaviour, the results are bound to the investigated flight state of 6° descent angle and 60 KTAS. Nevertheless, the extension and generalisation of the neural plant model and its properties in different directions is possible. By adding more network inputs like roll and pitch attitudes as well as flight

and descent variables, the system can be extended to other steady flight conditions (see Fig 10). Additionally, including the derivatives of these inputs allows the consideration of unsteady flight manoeuvres in the neural plant models.

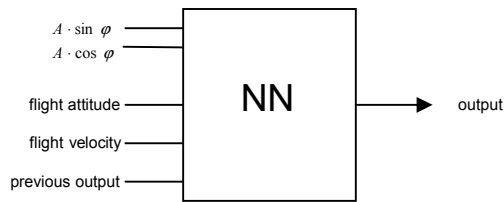


Fig 10: Extended neural network with additional inputs.

If necessary even pressure data of previous rotor revolutions can be added to the input vector in order to consider dynamic wake effects, resulting in an NNARX model (Neural Nonlinear AutoRegressive model with eXogenous Input). The investigations of all these approaches require appropriate training data for the set up of the neural networks and are therefore related to the availability of additional flight test data foreseen in the future.

4 Grey Box Approach

The intention of the grey box approach is to map the complex non-linear BVI plant by keeping its physical interpretability, allowing much easier localisation of mapping difficulties and failures. Additionally, existing knowledge about the BVI phenomenon can be used to provide a basic behaviour which supports the training process or just simplifies the complexity of the network functions, because only the unknown or uncertain parts of an existing model have to be taken into account. If the basic dynamic behaviour can be approximately described by a simplified model, the network component just has to learn the difference between measured data and model output preserving the dynamic functionality. In this case, less data samples are required for training.

For the grey box approach the idea of a convection model similar to prescribed vortex wake models is followed. These models prescribe the location of the blade tip vortices as a function of the wake age. From the predicted locations of the tip vortices, i.e. the parallelism of interaction as well as vertical miss distance, a BVI-Index will be derived, which is a measure for the generated noise.

In fact prescribed vortex wake models have been developed to enable predictions of the inflow through the rotor disk, however, these simple models which approximately describe the rotor wake geometry and the convection of the tip vortices are useful to introduce basic physical knowledge about BVI.

Beside models like “Rigid Wake” (trailed vortices are represented by skewed helical filaments) or “UTRC

Generalized Wake” (by Egolf & Landgrebe), the “Beddoes’ Generalized Wake Model” is of interest, since the trajectories of tip vortices are estimated with an assumption of the inflow distribution across the disk. The vertical displacement of the vortices is given by an integration of the inflow ratio over the wake age. This approach presents the use of a further kind of model, the inflow model. A basic inflow model was first suggested by Glauert (1926), followed by several variations (e.g. by Payne, Drees, White & Blake, Pitt & Peters, Howlett, Coleman) concerning the coefficients which describe the longitudinal and lateral distribution of the inflow (Ref 10).

A more sophisticated inflow model was developed by Mangler & Squire (1950, Ref 11). It uses the incompressible linearized Euler equation to relate the pressure field across the disk to an inflow distribution (Ref 10). This model was already involved in van der Wall’s work to predict the effect of active blade control on the vortex convection (Ref 12) and showed that it can yield an approximate description of the tip vortex locations near the rotor disk. Compared to free wake simulations (with CAMRAD II, Ref 13, including the CHARM Plugin, Ref 14) and measured BVI locations, the predictions based on Mangler’s inflow tend to lie in a similar region. For this reason the Mangler model is used as a basic model for the neural approach.

The neural convection model is divided in two main components (Fig 11), the planar and the vertical model. While the planar model describes the movements of the vortices in the plane of the blade tips (TPP), the vertical model maps the deflections perpendicular to it. Both are further divided into different modules explained in detail in sections 4.2 and 4.3.

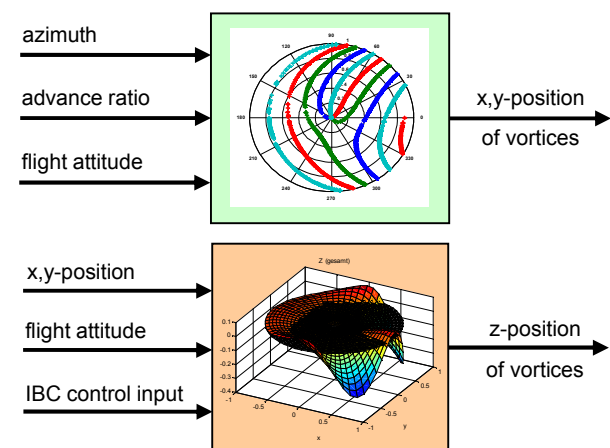


Fig 11: Two main components of the convection model, the planar model at the top, the vertical model below.

To adapt these components according to the in-flight measurements, the training data has to be prepared. This process is described in the following section.

4.1 Data Preparation

Modelling the vortex convection for the prediction of BVI noise, the point of interest is the position of the tip vortices in relation to the rotor blades. This information must be given by the training data but could not be measured directly in-flight. Additionally, regarding the experimental data, the existence of a tip vortex appears only in case of interactions with the blades. Therefore the measured blade pressure values are pre-processed to obtain the values needed for model training.

First, the model input values are extracted for each flight test series. In fact the nominal flight attitude was a 6° descent flight with an advance ratio of 0.15, deviations from this reference path occurred and are regarded as variable inputs. Second, the model output values, i.e. the locations of BVI events are computed in several steps.

The high frequent pressure coefficient fluctuations resulting from BVI are extracted by means of a wavelet filter (see Fig 12). Basically, the wavelet transformation serves as a high pass filter, but additionally enables the use of the wavelet coefficients to obtain information about the strength of interactions which could be included in a BVI index.

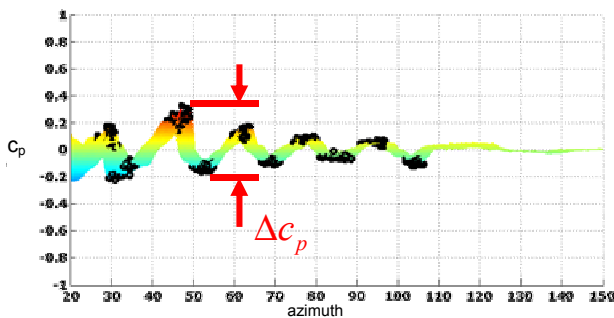


Fig 12: Fluctuations of the blade pressure coefficient (histories over several revolutions) resulting from BVI on the advancing side at a radius $r/R = 0,6$. The pressure rise ΔC_p for the interactions at 50° azimuth is marked.

The positions of interactions in the TPP can easily be found on the advancing side between a local maximum and minimum pressure coefficient (Fig 12), vice versa on the retreating side. The vertical distance of the vortices can only be estimated, which can be ascribed to two major problems. On the one hand, the vortex circulation strength is unknown and assumed to be approximately constant for the presented approach. On the other hand, observing only one interaction, it is not possible to decide whether the vortex was located above or below the rotor blade. Both cases lead to the same induced pressure jump.

According to investigations of Kitaplioglu, Caradonna and Burley a relation between the nominal vortex miss-distance and the BVI pressure rise ΔC_p was found for vortices with positive and

negative circulation (Fig 13, Ref 15). The authors assume that the dotted curve for the positive vortex generator incidence ($+12^\circ$) is probably erroneous. For that reason it is not taken into account.

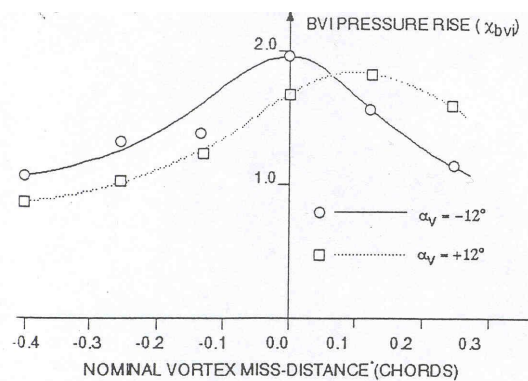


Fig 13: BVI pressure rise as a function of nominal vortex miss-distance (Ref 15) for different sense of vortex rotation.

For the estimation of the vortex distance based on the blade pressure data a function similar to the solid line in Fig 13 is used. However, the maximum pressure rise has to be modified, so that reasonable miss-distances occur. To accomplish this fact, the maximum pressure rise in the function is normalized with the maximum pressure rise in the measurements. Of course the vortex strength influences the height of the pressure jump, whereby an error is made in assuming constant vorticity.

To decide whether the vortex was above or under the TPP it is helpful to know that in the considered descent flight case the vortices first drift above, later below the TPP hitting the blades in the BVI relevant azimuth by about 40° to 80° (see Fig 14). Another important hint is that variations in the strength of interaction observed over many revolutions correlate for vortices on the same side of the TPP in contrast to vortices on different sides.

Based on this background a set of training data samples is extracted from the measurements of the different test series. The distributed locations found in one test series (Fig 14) are averaged over several revolutions resulting in vortex locations exemplarily shown in Fig 15.

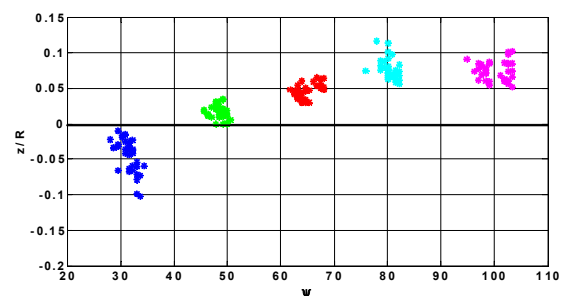


Fig 14: Estimated vertical vortex distances based on measurements at $r/R = 0,6$ over the rotor azimuth

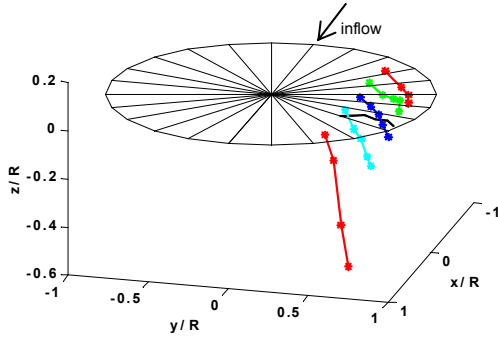


Fig 15: Estimated vortex locations based on measured interactions. The section with the TPP is marked.

At the moment only the advancing side as the main source of BVI noise is considered in the learning process, but no limitations exist to extend the models to the retreating side as well.

4.2 Planar Convection Model

For the planar convection model the following assumptions are made. The vortices are of constant strength and do not influence each other. They drift in x-direction according to the advance ratio μ , the lateral drift is neglected. Deviations resulting from the mentioned assumptions could be corrected by means of additional neural modules.

Basically the convection of the vortices is given similar to the prescribed wake models by the following equations

$$\begin{aligned} \frac{x_w}{R} &= r_{w0}(\psi) \cos \psi_{w0} + \mu \psi_{wa} = NN_{w0} + \mu \psi_{wa} \\ \frac{y_w}{R} &= r_{w0}(\psi) \sin \psi_{w0} = y_{w0} \end{aligned} \quad (4.1)$$

The vortices originate at the positions x_{w0} , y_{w0} , respectively r_{w0} , ψ_{w0} and drift with increasing wake age ψ_{wa} in x-direction. The main simplification is made in assuming that the vortex origin lies at a constant radius at the blade tip, because in the interesting regions from 90° to 270° azimuth they originate at varying radii just inboard the tip. For that reason a neural network module (Fig 16, marked with red letters in equation 4.1) maps the blade azimuth to the radius r_{w0} , and a lateral position y_{w0} to x_{w0} respectively. Thereby, the vortex generation radius is corrected so that the average of the measured positions can be predicted more exactly. The vortex origin surely depends on further variables like the pilot's and IBC inputs or flight attitudes, but this is not taken into account at the moment.

The NN has radial basis activation functions in the hidden layer and a linear output neuron. This network structure already shows good performance with about 10 radial basis neurons. Thus the

capability to consider further influences (inputs) is given and will be incorporated in the future.

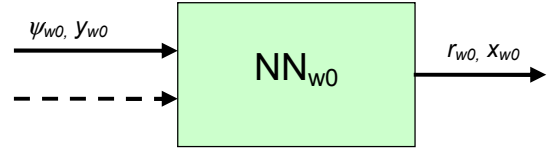


Fig 16: Neural network module to correct the vortex origin. Possible additional inputs are marked with the dashed arrow.

Two further neural correction modules have been investigated. The first one is an additional drift module (marked with red letters) for accounting unequal convection speeds according to the following equation

$$\begin{aligned} x_w &= x_{w0} + \mu \psi_{wa} + x_{varDrift} \\ &= NN_{w0} + x_{constDrift} + NN_{varDrift}(\psi_{wa}, y_w) \end{aligned} \quad (4.2)$$

The improvements offered by this component are quite small and can be neglected, additionally the computation of the vertical convection thereby would lead to a complicated integration over the inflow.

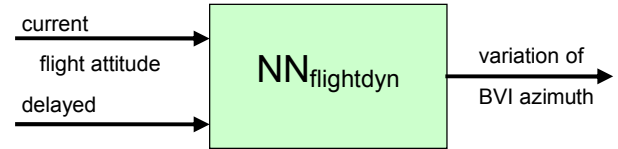


Fig 17: Feed forward network to map the dynamic variations of the azimuth of interactions.

The second correction module is a feed-forward network (Fig 17) to map the dynamic variations in the azimuth of the interactions observed over many revolutions. Primary investigations have shown that for an exemplary interaction the current and delayed flight attitudes can be mapped to the difference of the estimated (by Eq 4.1) and the measured interaction azimuth. The training process of this dynamic mapping requires data samples over a long time range i.e. many revolutions. For this reason a detailed validation of the neural model is the subject of current investigations.

4.3 Vertical Convection Model

As mentioned above, the vertical drift of the vortices can approximately be computed by an integration of the inflow distribution λ over the wake age according to the equation

$$\frac{z}{R} = -\mu_z \psi_{wa} + \int_0^{\psi_{wa}} \lambda_i d\psi \quad (4.3)$$

The entire inflow can be composed of two components, the downwash according to the flight attitude without active rotor control and the additional downwash resulting from the $2/rev$ IBC inputs (Fig 18). Furthermore the superposition is possible after the integration as well.

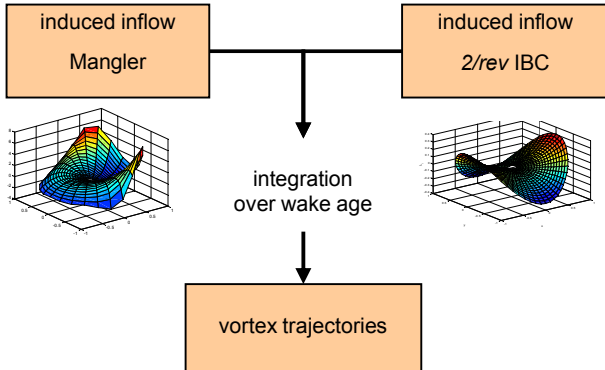


Fig 18: Two components of the vertical convection.

Since the training data samples are an estimation of the vortex positions, the z -component as a result from the integration should be used as model output. Assuming a constant convection speed in x -direction and no lateral drift, the integration over x instead of ψ_{wa} is possible. The resulting z -component for each x, y -coordinate in the TPP represents a 3D-surface on which the vortices drift.

For some simple induced downwash models the integration over x results in the following functional dependencies for the vertical deflections

$$\frac{z_i}{R} = -\frac{\lambda_{i0}}{\mu} \left[f_{Glauert}(x, x_{w0}, k_x) + f_{Drees}(x, x_{w0}, y, \mu) + f_{Beddoes}(x, x_{w0}, y, k_x) \right] \quad (4.4)$$

with $k_x(\mu, \lambda)$

The consideration of the functional dependencies is important for choosing the appropriate network topology. As can be seen, the integration starts at the vortex origin x_{w0} , resulting from the planar convection model. Since the Glauert downwash shows no variation in y , Drees allows lateral inequality and Beddoes indicates the vortex roll up. All are scaled with the induced inflow ratio and the advance ratio. The increasing inflow in longitudinal direction is described by k_x and depends on the flight attitude as well.

Except for Beddoes' model, these drift surfaces show no sufficient local characteristic so that the vortex convection could only be coarsely described in contrast to the surface based on the Mangler inflow model

$$\frac{z_i}{R} = -\frac{\lambda_{i0}}{\mu} \sum_{n=0}^{\infty} c_n a_n h_n(x, x_{w0}, y) \quad (4.5)$$

with $a_n = \sqrt{\frac{1 + \sin \alpha_{TPP}}{1 - \sin \alpha_{TPP}}}$, $c_n = const$

Thereby the shape of the drift surface is given by the form functions h_n scaled with the constant factors c_n and the factors a_n , which depend on the rotor inclination α_{TPP} . The form functions h_n are polynomials in x , x_{w0} and y and are derived in (Ref 12). Even if the Fourier series has infinite addends, n greater than 4 to 6 does not influence the surface significantly and is neglected here.

For adjusting the model to the prepared data samples a radial basis network is trained, which on the one hand maps the drift surface similar to Mangler and on the other hand adapts to the measured data in the BVI relevant region. To account for the influence of the flight attitude, the rotor inclination α_{TPP} is used as another input along with the longitudinal and lateral position

$$\frac{z_i}{R} = -\frac{\lambda_{i0}}{\mu} NN(x, y, \alpha_{TPP}, \dots) \quad (4.6)$$

Of course further inputs can be applied, such as the vortex origin x_0 , which is assumed to be constant for certain azimuths so far (see section 4.2).

The additional downwash resulting from the $2/rev$ IBC inputs is at present described by a model derived by van der Wall (Ref 12)

$$\begin{aligned} \frac{z_{IBC}}{R} &= -\frac{C_j}{\mu} \lambda_{i2} \sum_{i=2-m}^{2+m} \frac{A_{i2}}{A_2} \left[\cos(\varphi + \psi_{A_{i2}}) H_{2Cj} \right. \\ &\quad \left. + \sin(\varphi + \psi_{A_{i2}}) H_{2Sj} \right] \quad (4.7) \\ &= z_{IBC}(x, x_{w0}, y, \mu, \varphi, \psi_{A_{i2}}, A_2) \end{aligned}$$

The order of the induced radial velocity distribution is defined by C_j . The inflow λ_{in} by means of IBC is derived from the blade element theory and explained in detail in (Ref 12). The second part of the equations accounts for the m adjacent harmonics, which are excited by the $2/rev$ IBC inputs with the amplitude A_2 , the phase angle φ and the phase shift $\psi_{A_{i2}}$. The magnitude of the excited amplitudes is defined by A_{i2} . Presently no adjacent harmonics are considered because their influence is quite small and this model should be seen as an initial best guess for the network adaption.

Similar to the Mangler model, H_{2Cj} and H_{2Sj} are form functions in x , x_{w0} and y that define the shape of the drift surface. Due to the fact that dynamic inputs are higher harmonics of the rotor rotational frequency, the resulting additional inflow can be seen as periodical stationary waves over the rotor plane.

Additional simulations with the comprehensive rotor code CAMRAD II including the CHARM free wake model as plug-in (Ref 13, 14) support the investigation of the IBC influence on the vortex trajectories. They show similar results to the above mentioned model.

The two components of the vertical convection model are illustrated in Fig 19. Both depend on the flight attitude. The adaption of the neural model for the IBC influence with the measured data is subject

of the current work. Results from the neural model for the descent (reference) flight are presented in the following section.

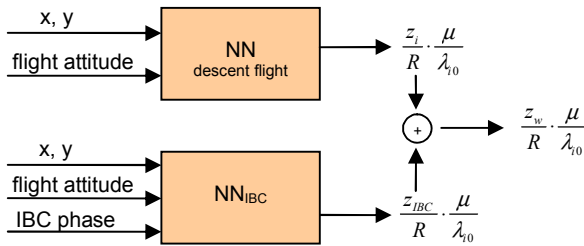


Fig 19: Neural network modules to describe the vertical convection.

4.4 Results and Discussion

In the case of the planar convection model the estimation of the BVI locations can be essentially improved by means of the network module which corrects the vortex origin, as compared in Fig 20. Thereby only one test series is considered.

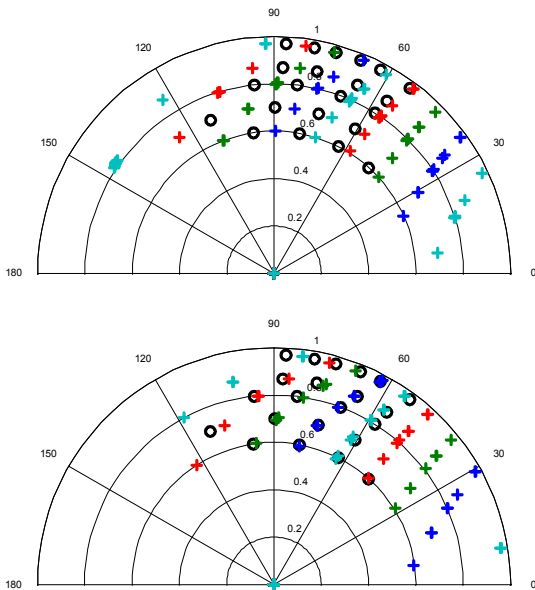


Fig 20: Comparison of the planar convection model without (above) and with (below) NN_{w0} correction. Measured locations are marked by 'o', model outputs by '+'.
(Note: The caption text in the image contains a typo: 'o' instead of '+')

Taking several test series with slightly different flight paths into account, small variations of the measured locations arise since only a mean position can be mapped without further inputs. For this reason future work will incorporate this subject, particularly when larger variations from the reference flight path are considered. These variations have to be distinguished from smaller dynamic variations observed over several rotor revolutions. Therefore the neural network module $NN_{flightdyn}$ will be used.

The vertical model for the descent flight without IBC according to equation 4.6 is a neural network with

radial basis activation functions in the hidden layer and one linear output neuron. At first, only one test series and thus no influence of the flight attitude are considered (Fig 21). The appropriate radial basis network has 22 hidden neurons.

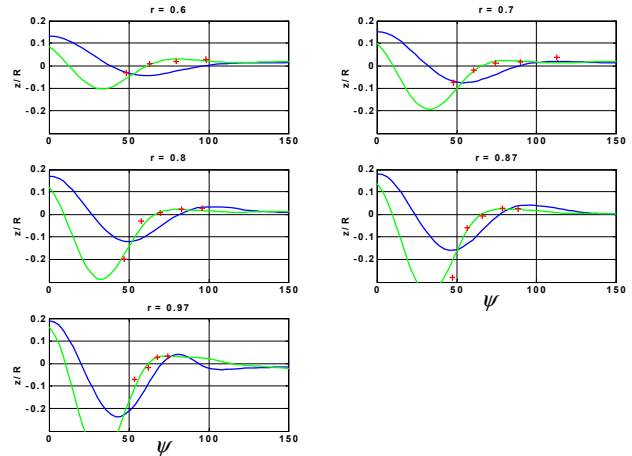


Fig 21: The neural model (green line) in comparison to its Mangler basis (blue line) and the estimations from the measured locations (red +). The vertical distance is plotted over the rotor azimuth (advancing side) for the radii with the Kulites

The network shows good adaptability towards the training data samples without losing the basic shape. In Fig 21 just the sections with the radial positions where the measurements were made are presented. The mapping quality can be tested with input data from regions which are not covered by the training data. The neural model output over the whole input range is illustrated in Fig 22, once again compared with the prediction based on Mangler's inflow and the prepared measurements. It shows that plausible network outputs are not restricted to the area defined by the measured data only, because the data used for the training process was supported by the existing Mangler model.

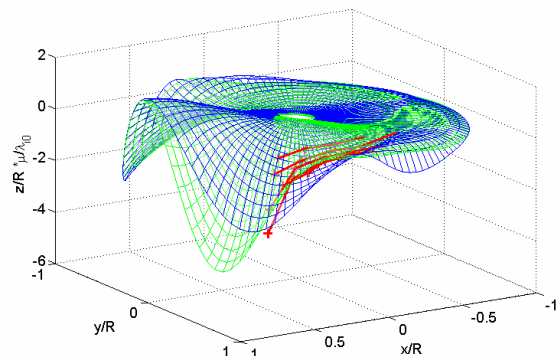


Fig 22: The neural model (green mesh) in comparison to its Mangler basis (blue mesh) and the estimations from the measured locations (red)

Further on, the neural model was adapted to several test series with slightly different flight attitudes, which is considered by the inclination of the TPP as

an additional network input. Again, the network adapts quite well and indicates remarkable sensitivity concerning the additional input (Fig 23). The number of neurons in the hidden layer of the radial basis network increases to 32. Of course, it is imaginable that further dependencies exist, which need to be thoroughly investigated in the future.

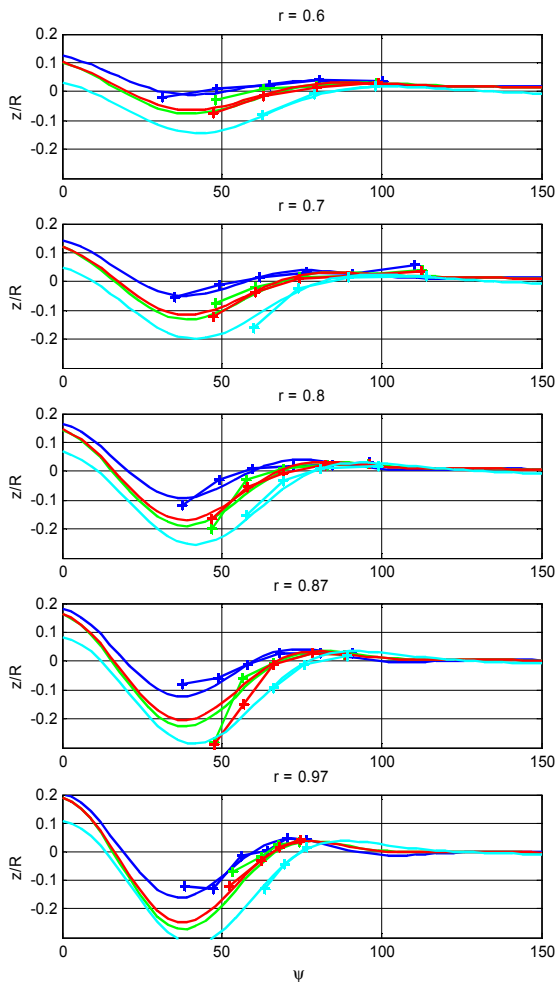


Fig 23: Sections of the drift surfaces for different α_{TPP} , one colour for each test series. Neural model outputs (solid lines) are compared with the estimations from the measurements(+).

The main information extracted from these results is the location of the section of the drift surface with the TPP. In combination with the planar model output, enough clues should be available from there to derive BVI noise indices which could serve as a feedback for the noise controller.

5 Summary

The aim of the neural network approaches is to identify the non-linear dynamic BVI system for the use as a plant model in a future real time BVI noise controller. Due to the extensive flight test data and the non-linear behaviour, a data driven design with neural networks is convenient.

The black box approach maps the measured blade pressure values for a steady descent with different IBC inputs. The derived BVI index evaluates the predicted pressure signals concerning the occurring interactions. Different network structures are investigated and are able to reproduce the measurements very well.

The alternative grey box approach maps the estimated vortex locations depending on the flight attitude and is divided in several components. The networks show good adaptability towards the prepared data samples, though further model dependencies have to be investigated. The intention of this kind of modelling is not, to achieve the accuracy of specific BVI codes, but to predict the approximate influence of IBC inputs on BVI as a basis for control design.

Both approaches emphasise the generalisation capability of the neural models to reasonably predict the plant behaviour in input regions not explicitly included in the training process.

Based on the identified neural plant models a closed loop BVI controller will be designed. Due to the non-linearity of the BVI system a neural controller design is considered, even though a conventional approach becomes possible as well.

Acknowledgements

The authors as well as both institutions, the "Institut für Statik und Dynamik der Luft- und Raumfahrtkonstruktionen (ISD), Universität Stuttgart", and the Eurocopter Deutschland GmbH (ECD), Munich, acknowledge the financial support of essential parts of this work by the German Federal Ministry of Education and Research (BMBF), Bonn, under grant number 13N8058. This includes the financial project management service provided by Dr. Hoffschulz from the "Verein Deutscher Ingenieure" (VDI), Düsseldorf, in the framework of this programme.

References

- [1] Splettstößer W.R., Schultz, K.-J., Kube, R., Brooks, T.F., Booth, E.R, Niesl, G., Streby O.: BVI impulsive noise reduction by higher harmonic pitch control: Results of a scaled model rotor experiment in the DNW, 17th European Rotorcraft Forum, September 1991
- [2] Swanson, S.M., Jacklin, S.A., Blaas, A., Kube, R., Niesl, G., Individual blade control effects on blade vortex interaction noise, 50th Annual Forum of the American Helicopter Society, Washington D.C., May 1994

- [3] Schoell, E., Gembler, W., Bebesel, M., Spletstößer, W., Kube, R., Pongratz, R., Noise reduction by blade root actuation – analysis of flight and wind tunnel tests, 24th European Rotorcraft Forum, Marseille, September 1998
- [4] Roth, D., Dieterich, O., Bebesel, M., Pongratz, R., Kube, R., Munser, H., Individual blade root control demonstration – recent activities, 27th European Rotorcraft Forum, Moscow, September 2001
- [5] Rojas, R., Theorie der neuronalen Netze, Springer Verlag, Berlin, 1996, 4. korrigierter Nachdruck
- [6] Demuth, H., Beale, M., MATLAB, Neural Network Toolbox User's Guide, Natick, 1998, Version 3
- [7] Nørgaard, M., Ravn, O., Poulsen, N.K., Hansen, L.K., Neural Networks for Modelling and Control of Dynamic Systems, Springer Verlag, London, 2000
- [8] Rudolph, S., On Topology, Size and Generalization of Non-linear Feed-Forward Neural Networks, Neurocomputing, vol. 16, no. 1 (July 1997), pp. 1-22.
- [9] Andres, S., Impulslärm-Analyse bei Hubschraubern mit der Wavelet-Transformation, Diplomarbeit, TU Berlin, November 1998
- [10] Leishman, J.G., Principles of Helicopter Aerodynamics, Cambridge University Press, Cambridge, 2000
- [11] Mangler, K.W., Squire, H.B., The Induced Velocity Field of a Rotor, Aeronautical Research Council Technical Reports and Memoranda No. 2642, England, 1950
- [12] van der Wall, B.G., Der Einfluß aktiver Blattsteuerung auf die Wirbelbewegung im Nachlauf von Hubschrauberrotoren, DLR Forschungsbericht 1999-34, Braunschweig, 1999
- [13] Johnson, W., Technology Drivers in the Development of CAMRAD II, AHS Aeromechanics Specialists Conference, San Francisco, California, January 19–21, 1994
- [14] Wachspress, D., CHARM PLUGIN to CAMRAD II Version 2.2c User's Manual, Continuum Dynamics, Inc., Princeton, New Jersey, October 2002
- [15] Kitapliglu, C., Caradonna, F.X., Burley, C.L., Parallel Blade-Vortex Interactions: An Experimental Study and Comparison with Computations, American Helicopter Society 2nd International Aeromechanics Specialists' Conference, Bridgeport, CT, October 11-13, 1995